agronomy

MDPI

Article

Adsorption Properties of Fishbone and Fishbone-Derived Biochar for Cadmium in Aqueous Solution

Nan Pei [1,2], Wenwen Luo [1,2], Qingqing Huang [1,2,*] and Yuebing Sun [1,2]

[1] Key Laboratory of Original Agro-Environmental Pollution Prevention and Control, Ministry of Agriculture and Rural Affairs (MARA), Agro-Environmental Protection Institute, MARA, Tianjin 300191, China; upllink4n@gmail.com (N.P.); sk7n07@gmail.com (W.L.); sunyuebing@aepi.org.cn (Y.S.)

[2] Tianjin Key Laboratory of Agro-Environment and Agro-Product Safety, Agro-Environmental Protection Institute, MARA, Tianjin 300191, China

* Correspondence: huangqingqing@caas.cn; Tel.: +86-176-0220-9636

Abstract: Cadmium (Cd) contamination in aquatic ecosystems is a serious global environmental issue. Biochar derived from agricultural wastes has recently attracted remarkable attention as it is used as an absorbent in combating heavy metal contamination of water bodies. In the present study, the absorption efficacy of fish bone (FBM) and fishbone-derived biochar prepared at 200 °C, 400 °C, 600 °C, and 800 °C (referred to as B_{200}, B_{400}, B_{600}, and B_{800}, respectively) for the Cd ion (Cd^{2+}) in aqueous solution was investigated. The results showed that high-temperature pyrolysis could optimize the pore structure and specific surface area of FBM, and Cd^{2+} successfully adsorbed onto FBM and fishbone-derived biochar. High-temperature pyrolysis significantly increased the FBM adsorption capacity for Cd^{2+} by 49.5–135.1%, with the optimal pyrolysis temperature being 600 °C. Furthermore, the kinetic data of FBM and fishbone-derived biochar for Cd^{2+} were in better alignment with the pseudo-second-order model, their adsorption isotherms were better in accordance with the Langmuir models, and the thermodynamic analysis showed that the adsorption process was monolayer and favorable adsorption. Moreover, the potential adsorption mechanisms of Cd^{2+} on FBM and fishbone-derived biochar might be related to pore filling, ion exchange, complexation with oxygen functional groups, and precipitation with the minerals on the biochar surface. Fishbone-derived biochar has significant potential for wastewater treatment and agricultural waste applications.

Keywords: adsorption properties; biochar; cadmium; fishbone

Citation: Pei, N.; Luo, W.; Huang, Q.; Sun, Y. Adsorption Properties of Fishbone and Fishbone-Derived Biochar for Cadmium in Aqueous Solution. *Agronomy* **2024**, *14*, 2717. https://doi.org/10.3390/agronomy14112717

Academic Editor: Baskaran Stephen Inbaraj

Received: 18 October 2024
Revised: 13 November 2024
Accepted: 15 November 2024
Published: 18 November 2024

1. Introduction

Heavy metal pollution in aquatic ecosystems is a serious global environmental issue and has attracted considerable attention in recent years [1]. Heavy metals are widely utilized throughout numerous industries, such as electroplating, smelting, mining, battery manufacturing, textile printing, and leather making [2]. Industrial wastewater, exhaust emissions, and solid waste discharges result in serious heavy metal contamination in aquatic ecosystems [3,4]. Among heavy metals, cadmium (Cd) is one of the most toxic and widespread pollutants in the environment [5]. As a hazardous heavy metal, Cd is not an essential component for living organisms, and Cd that accumulates in the food chain poses a significant threat to humans, animals, and the ecosystem [6]. Consequently, it is essential to use effective technologies to eliminate Cd ions from Cd-contaminated wastewater prior to its discharge into the environment.

Various technologies have been developed to remediate water contaminated with heavy metals due to the indiscriminate release of heavy metals into aquatic environments; these include chemical precipitation, ion exchange, adsorption, coagulation, oxidation, reduction, membrane separation, and reverse osmosis technologies [7]. Among these technologies, adsorption is the most frequently used technology for removing heavy metal ions from the contaminated water due to its ease of operation, high efficiency, low cost,

and low secondary pollution. Materials such as carbonaceous materials, zeolites, clays, composite materials, polymeric materials, and biochar with good adsorption performance are widely used as heavy metal adsorbents [6–8]. Of these, biochar derived from agriculture wastes (i.e., crop straw, shell, and livestock manure) has recently received remarkable attention for its application as an absorbent in sewage treatment [9,10]. Biochar has a high adsorption capacity for heavy metals owing to its large specific surface area, porous structure, strong cation exchange capacity, and various functional groups [11,12]. For instance, biochar derived from pyrolyzed rice husk at 700 °C had a maximum adsorption capacity of 93.50 mg·g^{-1} for Cd^{2+} [13], and pinecone biochar had an adsorption capacity of up to 92.7 mg g^{-1} [1]. Overall, using biochar as an absorbent to remove heavy metal ions from wastewater has the potential for wide applications. Furthermore, the use of agricultural waste-derived biochar as an absorbent for the removal of heavy metal ions benefits not only wastewater treatment but also enhances agricultural waste recycling [9].

In recent decades, the aquaculture industry has been expanded significantly worldwide, and China is currently the world's largest producer of aquatic products [14]. Among the aquatic products, fish ranks as one of the most traded aquatic commodities globally, with significant growth in both production and consumption in recent years [15]. Fish and fish products serve as vital nutritional supplies for humans, being abundant in high-quality protein, unsaturated fatty acids, and specific minerals and vitamins [16]. However, along with the fast growth in fish production, the fish processing industry produces vast amounts of byproducts. Fishbone, while being rich in calcium, has frequently been discarded directly as the primary by-product without any additional transformation into value-added products [17,18]. Thus, appropriate treatment or utilization is a requirement to minimize this waste and mitigate environmental pollution.

Natural fishbone is a low-cost natural material composed roughly of 70% mineral components (mainly hydroxyapatite (HAP)) and 30% organic constituents (primarily fibrous protein collagen) [19]. Previous research has demonstrated that HAP is an efficient adsorption material due to its high removal capability for heavy metals through an ion-exchange reaction with calcium ions on the bone surface [20]. In addition, multiple studies showed that biochar derived from fishbone has outstanding adsorption effects on heavy metal ions (e.g., copper, cobalt, nickel) in aqueous solutions [21]. However, very little work has been conducted on the efficacy of fishbone biochar for Cd^{2+} removal from aqueous solutions.

The present study focuses on the usage of fishbone (FBM) and fishbone-derived biochar obtained at different pyrolysis temperatures to test their capacity for Cd^{2+} removal from aqueous solutions. Furthermore, the effect of different environmental parameters, such as pH and initial Cd^{2+} concentration, on Cd^{2+} absorption by fishbone and fishbone-derived biochar was investigated; the role of functional groups on the absorption of Cd^{2+} by FBM and fishbone-derived biochar was studied using Fourier transform infrared (FTIR). We anticipate that the current study will give a scientific basis for the efficient remediation of heavy metal contamination in aquatic ecosystems with FBM and open up new avenues for the rational development and recycling of fishbone.

2. Materials and Methods

2.1. Chemical Reagents

The used chemicals, such as nitric acid (HNO_3), potassium nitrate (KNO_3), sodium hydroxide (NaOH), and others, were purchased from the Tianjin Chemical Reagent Co., Ltd., Tianjin, China, and were all of the reagent grade. Deionized water (18.2 MΩ/cm, Milli-Q) was used to prepare the chemical solution and rinse the samples. The specific concentration of Cd^{2+} solution was prepared using cadmium (Cd) nitrate tetrahydrate ($Cd(NO_3)_2{\cdot}4H_2O$) and adjusted to different pH values with 0.1 mol·L^{-1} HNO_3 and NaOH solutions.

2.2. Preparation of Fishbone and Fishbone-Derived Biochar

The fishbone collected from the fishing market of Tianjin, China, was washed with deionized water and then oven-dried at 105 °C to obtain constant samples. The oven-dried

fishbone was further grounded and sieved to achieve a particle size of 0.15 mm for the pyrolysis process, and the resulting powder was referred to as FBM. Afterwards, a portion of the FBM samples was pyrolyzed in a muffle furnace at 200 °C, 400 °C, 600 °C, and 800 °C for 3.5 h under a nitrogen (N_2) atmosphere. The resultant biochar was referred to as B_{200}, B_{400}, B_{600}, and B_{800}, respectively. The biochar was then homogenized and screened to pass through a 0.15 mm sieve.

2.3. Characterization of Fishbone and Fishbone-Derived Biochar

The thermogravimetric analysis (TGA) of FBM was performed using TA instruments TGA/SDT Q600 equipment (TA, Instrument, New Castle, DE, USA). The measurements were conducted in a N_2 atmosphere with a heating rate of 10 °C ·min^{-1}, ranging from 20 °C to 700 °C. The specific surface area and pore volume of FBM and fishbone-derived biochar (B_{200}, B_{400}, B_{600}, and B_{800}) were measured using a specific surface area analyzer (Quadrasorb Si, Quanta Instruments, Inc., Boynton Beach, FL, USA) with the Brunauer–Emmett–Teller (BET, MicrotracBEL BELSORP-max, Tokyo, Japan) and Barret–Joyner–Halenda (BJH) method. The functional groups of FBM and fishbone-derived biochar (B_{200}, B_{400}, B_{600}, and B_{800}) were determined by Fourier transform infrared spectroscopy (FTIR) (Tensor 37, Bruker Corporation, Karlsruhe, Germany), with a spectrum range of 400–4000 cm^{-1} with a resolution of 1 cm^{-1}. The morphologies and elemental distributions of FBM and fishbone-derived biochar (B_{200}, B_{400}, B_{600}, and B_{800}) were investigated using a scanning electron microscope with energy dispersive spectroscopy (SEM–EDS, SU3500i, Hitachi, Tokyo, Japan). The point of zero charge of FBM and fishbone-derived biochar (B_{200}, B_{400}, B_{600}, and B_{800}) was measured following the modified pH drift method [22]. In brief, 0.1 g of FBM and fishbone-derived biochar (B_{200}, B_{400}, B_{600}, and B_{800}) were added into the centrifuge tube with 50 mL of 0.01 M $NaNO_3$ solution at different pH values and mixed. The initial pH value of solution was adjusted to 3–12 with 0.1 M HNO_3 and NaOH solutions. Thereafter, the suspensions were oscillated at 25 °C for 24 h, and the final pH values were determined by a pH meter (PB-10, Sartorius, Gottingen, Germany). The pHpzc corresponds to the pH value where the curve crosses the line of $pH_{initial} = pH_{final}$. The crystal structures of the FBM and fishbone-derived biochar (B_{200}, B_{400}, B_{600}, and B_{800}) were determined by X-ray diffraction (XRD, D8 Advance, Bruker, Saarbrucken, Germany), with scans conducted over a diffraction angle range of 10° to 90° at a scanning speed of 4°·min^{-1}.

2.4. Adsorption Experiments

Adsorption kinetic experiments were conducted in 2000 mL conical flasks. First, 10 g of FBM or fishbone-derived biochar (B_{200}, B_{400}, B_{600}, and B_{800}) was added to a 500 mL solution containing an initial Cd^{2+} concentration of 200 mg·L^{-1} and a pH of 5.40. The mixture was then stirred with a magnetic stirrer at a speed of 400 rpm and 25 °C for 12 h. The mixture was sampled at different intervals (0, 2, 5, 10, 20, 40, 60, 120, 180, 360, 480, and 720 min). The resultant solution was filtered through a 0.45 μm water filter membrane, and the Cd concentration in filtrate was measured using a flame atomic absorption spectrophotometer (FAAS, ZEEnit 700P, Jena Analytical Instrument Co., Ltd., Thuringia, Germany).

Adsorption isothermal experiments were performed in a series of 50 mL conical flasks containing 0.05 g of FBM or fishbone-derived biochar (B_{200}, B_{400}, B_{600}, and B_{800}) and 25 mL of Cd^{2+} solution with different initial concentrations (at pH 5.40). The conical flasks were then shaken at 200 r·min^{-1} in a thermostat oscillating chamber (ZHWY-2102C, Shanghai Zhicheng analytical Instrument Manufacturing Co., Ltd., Shanghai, China) for 12 h under 25 °C. The resulting solution was filtered through a 0.45 μm water-based filter membrane, and the Cd concentration in the filtrate was measured by FAAS.

The effect of pH on the adsorption performance of Cd^{2+} by FBM and fishbone-derived biochar was investigated in a series of 50 mL conical flasks. Each conical flask contained 0.05 g of FBM or fishbone-derived biochar (B_{200}, B_{400}, B_{600}, and B_{800}) and 25 mL of Cd^{2+} solution with an initial concentration of 100 mg·L^{-1} adjusted to a pH range of 3–8 by adding 0.1 mol·L^{-1} NaOH or 0.1 mol·L^{-1} HNO_3 solutions. The conical flasks were then

shaken at 200 r·min^{-1} in a thermostat oscillating chamber for 30 min. After adsorption, the solution was filtered through a 0.45 μm filter, and the Cd concentration in suspension was determined by FAAS.

2.5. Analysis Methods

The adsorption capacity of the adsorbent for Cd^{2+} was calculated using Equation (1) as follows:

$$q_e = \frac{(C_0 - C_t) \times V}{m} \quad (1)$$

where C_0 and C_t represent the initial concentration (mg·L^{-1}) of Cd^{2+} in solution and the concentration (mg·L^{-1}) of Cd^{2+} in solution at the time of adsorption t (min), respectively; V is the volume of solution (L); and m is the mass of adsorbent (g).

The experimental data for adsorption kinetics of Cd^{2+} onto absorbent were fitted using the pseudo-first-order model as Equation (2) and the pseudo-second-order model as Equation (3), as shown below:

$$\frac{dq_t}{dt} = k_1(q_e - q_t) \quad (2)$$

$$\frac{dq_t}{dt} = k_2(q_e - q_t)^2 \quad (3)$$

where q_t represents the amount of Cd^{2+} adsorbed at time t (mg·g^{-1}); q_e represents the amount of Cd^{2+} adsorbed at equilibrium (mg·g^{-1}); and k_1 (min^{-1}) and k_2 (g·mg^{-1}·h^{-1}) are pseudo-first-order adsorption and pseudo-second-order adsorption rate constants, respectively.

The experimental data for the adsorption isotherms for Cd^{2+} removal from solution by absorbent were fitted using the Langmuir and Freundlich models, as indicated in Equations (4)–(6), respectively:

$$q_e = \frac{Q_m K_L C_e}{1 + K_L C_e} \quad (4)$$

$$q_e = K_F C_e^{\frac{1}{n}} \quad (5)$$

$$R_L = \frac{1}{1 + K_L C_e} \quad (6)$$

where q_e represents the adsorption amount of Cd^{2+} (mg·g^{-1}) at equilibrium; Q_m represents the adsorption constant; C_e represents the Cd^{2+} concentration at equilibrium (mg·L^{-1}); K_L (L·mg^{-1}) and K_F (mg·g^{-1}) represent adsorption parameters of the Langmuir and Freundlich models, respectively; $1/n$ represents the Freundlich dimensionless parameter; and R_L represents the separation factor of the Langmuir model.

All treatments were replicated in triplicate in the experiments. The statistical analysis utilized SAS 9.0 and Origin 2019, with the results expressed as mean ± SD (standard deviation of means).

3. Results and Discussion

3.1. Characterization of Fishbone and Fishbone-Derived Biochar

Figure 1a depicts the thermal stability of the fishbone (FBM) examined by TGA/DTG, and there are three distinct weight-loss stages with a maximum mass loss of 44.80%. The first weight-loss stage (3.80%) occurs between 9 °C and 146.42 °C, attributed to the evaporation of adsorbed water in the FBM sample. At this stage, the DTA curve reaches an endothermic peak at 49.13 °C. The second weight loss stage (27.10%) occurs around 146.42–538.83 °C with the endothermic peak on the DTA curve appearing at 318.06 °C. Mass loss in the second stage was attributed to collagen decomposition, which was driven by the degradation of several compounds rather than a single component. Furthermore, at this stage, the decomposition of C-H, C-O, and C-C bonds mostly led to the formation of H_2O, CO, CO_2, and other decomposition products of simple alkane compounds. The

third stage of weight loss (12.89%) occurs in the region of 538.83–733.41 °C as a result of the decomposition of the remaining organic compounds and the re-decomposition of the intermediates formed during collagen decomposition. The endothermic peak appears at 677.47 °C on the DTA curve. Further, above 733.41 °C, there is a slight mass loss (0.98%) due to the decomposition of carbonate [19,23].

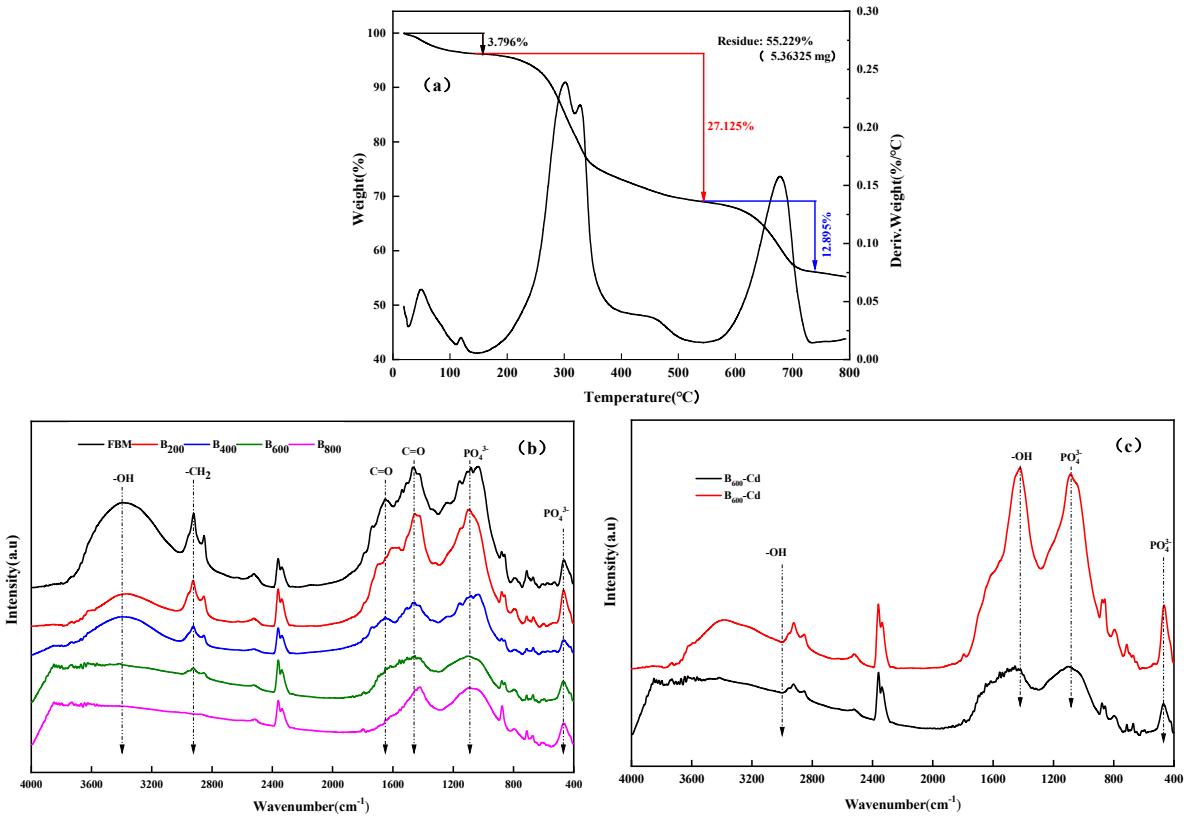

Figure 1. The DTA/TGA analysis of fish bone powder at different heating rates (**a**); FTIR spectra of fishbone and fishbone biochar (**b**); and Cd-absorbed biochar (**c**). FBM represents fishbone; B_{200}, B_{400}, B_{600}, and B_{800} represent fishbone biochar prepared at 200 °C, 400 °C, 600 °C, and 800 °C, respectively; B_{600}-Cd represents Cd-absorbed biochar prepared at 600 °C.

Fourier transform infrared (FTIR) spectra were employed to identify the characteristic peaks of different ligands in FBM, fishbone-derived biochar, and Cd-absorbed biochar. According to Figure 1b, the broad absorption peaks observed between 3800 cm^{-1} and 3000 cm^{-1} represent -OH stretching vibration; the peaks at 2924 cm^{-1} and 2853 cm^{-1} are associated with $-CH_2$ vibration; the peaks at 1650 cm^{-1} and 1460 cm^{-1} correspond to the carbonyl (C=O); the peaks at 1090 cm^{-1} and 470 cm^{-1} represent the symmetric stretching vibrations of phosphate (PO_4^{3-}) groups. Moreover, the -OH peak at 3396 cm^{-1} and the PO_4^{3-} peak at 1090 cm^{-1} indicate the presence of hydroxyl calcium phosphate (HAP) in FBM [4,23]. Furthermore, it is immediately apparent that the morphologies of the FTIR spectra shift as the pyrolyzed temperature rises. With the increase in pyrolyzed temperature, the broad absorption peaks between 3800 cm^{-1} and 3000 cm^{-1} vanished; these belonged to water molecules and hydrogen-bonded hydroxyl and are consistent with those of previous studies [4]. The peaks at 2924 cm^{-1} and 2853 cm^{-1} gradually disappeared, and the intensity of peaks at 1460 cm^{-1} significantly decreased, while a new series of peaks emerged in the absorption spectra, indicating that the structure of FBM was altered by high-temperature pyrolysis. It can be attributed to the following reasons: First, the carbonation and aromatic structure of biochar increase with increasing pyrolyzed temperature, while oxygen-containing functional groups decrease [24,25]; Second, the high-temperature carbonization process might cause the condensation of hy-

droxyl groups in FBM. The FTIR spectra of fishbone-derived biochar (B_{200}, B_{400}, B_{600}, and B_{800}) showed that the intensity of peaks at 1090 cm^{-1} and 1030 cm^{-1} increased with the increased pyrolysis temperature, and these two peaks merged at 1030 cm^{-1} in the FTIR spectra of B_{600} and B_{800} samples, which was due to the C-O decomposition or overlap caused by C-O displacement above 400 °C. Moreover, a comparison of the FTIR spectra of B_{600} and Cd-absorbed biochar (B_{600}-Cd) showed a significant increase in the intensity of peaks at 3200 cm^{-1}, 1460 cm^{-1}, 1090 cm^{-1}, and 470 cm^{-1} (Figure 1c), indicating the critical role of -OH and PO_4^{3-} functional groups on the biochar surface for Cd^{2+} adsorption, while other carbon-containing functional groups also contribute significantly to the Cd^{2+}-removal process.

Figure 2 depicts the pore structure parameters of FBM and fishbone-derived biochar (B_{200}, B_{400}, B_{600}, and B_{800}). Generally, the N_2 adsorption–desorption isotherms of B_{400}, B_{600}, and B_{800} exhibited a typical IV-type adsorption isotherm with a distinct type H3 hysteresis loop in the relative pressure range of 0.2–0.9, indicating the existence of the mesoporous structures. Additionally, pronounced hysteresis was observed in the relative pressure range from 0.4 to 0.9, suggesting the existence of mesopores and macropores in B_{400}, B_{600}, and B_{800} samples. When the relative pressure exceeded 0.9, the adsorbed volume rapidly increased, indicating the presence of a certain number of macropores in B_{400}, B_{600}, and B_{800} samples. Furthermore, this was confirmed by the corresponding pore size distribution curves of FBM and fishbone-derived biochar (Figure 2b). The pore volumes of FBM increased significantly as the pyrolyzed temperature increased. Moreover, the pore volumes of FBM and fishbone-derived biochar (B_{200}, B_{400}, B_{600}, and B_{800}) were 0.004 $cm^3 \cdot g^{-1}$, 0.007 $cm^3 \cdot g^{-1}$, 0.007 $cm^3 \cdot g^{-1}$, 0.014 $cm^3 \cdot g^{-1}$, and 0.014 $cm^3 \cdot g^{-1}$, respectively, with average pore diameters of 4.81 nm, 4.68 nm, 15.27 nm, 19.97 nm, and 23.33 nm, respectively.

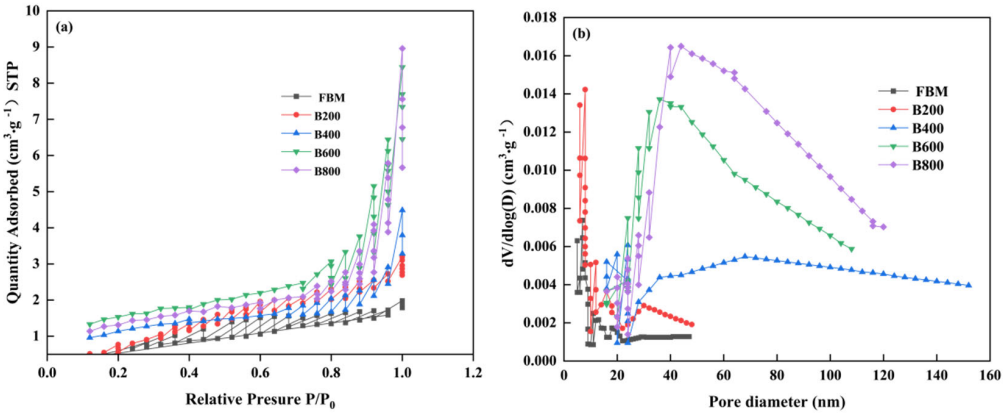

Figure 2. The N_2 adsorption–desorption isotherms (**a**) and pore size distribution of fishbone and fishbone biochar (**b**). FBM represents fishbone; B_{200}, B_{400}, B_{600}, and B_{800} represent fishbone biochar prepared at 200 °C, 400 °C, 600 °C, and 800 °C, respectively.

The Brunauer–Emmett–Teller (BET) analysis showed that the specific surface area of fishbone-derived biochar increased by 83.25% as the pyrolysis temperature increased from 0 °C to 200 °C (Table 1). This occurred because at this stage, the breakdown of collagen leads to the formation of high-density structures with small surface areas, resulting in an increase in specific surface areas. Previous research has demonstrated that the functional groups generated on biochar during the pyrolysis process at temperatures ranging from 200 °C to 400 °C would block the micropores, leading to a decrease in surface area [7]. Furthermore, when the pyrolysis temperature was further increased from 600 °C to 800 °C, crystal growth might occur, which is typically accompanied by a further decrease in surface area [19]. Overall, the above findings indicated that high-temperature pyrolysis could optimize the pore structure and specific surface area. In addition, the pH_{ZPC} values of fishbone-derived biochar increased as the pyrolysis temperature increased, particularly for B_{600} and B_{800}. The pH_{pzc} of B_{600} and B_{800} was significantly increased by 3.39 and 4.73,

respectively, as compared with that of FBM. This indicated that biochar prepared at high pyrolysis temperature had more surface positive charges, which was consistent with the research of Sun et al. [22].

Table 1. The parameters of surface area, pore volume, pore diameter, and point of zero charge (pH_{ZPC}) of fishbone and fishbone-derived biochar.

Sample	Surface Area ($m^2 \cdot g^{-1}$)	Pore Volume ($cm^3 \cdot g^{-1}$)	Average Pore Diameter (nm)	pH_{ZPC}
FBM	2.274	0.004	4.811	6.05
B_{200}	4.159	0.007	4.678	6.40
B_{400}	1.651	0.007	15.27	6.95
B_{600}	2.855	0.014	17.97	9.44
B_{800}	2.472	0.014	22.33	10.78

Note: FBM represents fishbone; B_{200}, B_{400}, B_{600}, and B_{800} represent fishbone biochar prepared at 200 °C, 400 °C, 600 °C, and 800 °C, respectively.

Table 2 presents the element compositions of fishbone and fishbone-derived biochar determined by SEM–EDS. The primary elements of FBM and fishbone-derived biochar include phosphorus (P), sulfur (S), and chloronium (Cl), along with trace amounts of other elements, such as potassium (K) and calcium (Ca), with the highest Ca contents observed in B_{600} and B_{800} samples (Table 2). Given that FBM and fishbone-derived biochar were rich in Ca and P, we hypothesize the presence of calcium hydroxyapatite ($Ca_{10}(PO_4)_6(OH)_2$) in these materials.

Table 2. Element compositions of fishbone and fishbone-derived biochar determined by SEM–EDS.

Element ($mg \cdot kg^{-1}$)	FBM	B_{200}	B_{400}	B_{600}	B_{800}
Ca	16.79	16.64	16.59	17.32	24.84
P	9793.90	9622.82	13,117.19	11,895.36	10,486.47
K	1.06	1.08	1.19	1.20	1.18
Na	0.81	0.78	ND	ND	1.63
Mg	1.24	1.23	2.26	2.77	3.68
S	5980.80	6016.09	6651.71	6394.74	6113.43
Cl	78,805.95	80,596.73	102,077.70	105,665.70	68,138.16
Cd	ND	ND	ND	ND	ND

Note: ND means no detection. FBM represents fishbone; B_{200}, B_{400}, B_{600}, and B_{800} represent fishbone biochar prepared at 200 °C, 400 °C, 600 °C, and 800 °C, respectively.

3.2. Adsorption Performance

3.2.1. Adsorption Kinetics

The kinetics of Cd^{2+} adsorption onto FBM and fishbone-derived biochar were analyzed using the pseudo-first-order and pseudo-second-order models, as shown in Figure 3a and Table 3. The adsorption capacity of Cd^{2+} by FBM and fishbone-derived biochar increased rapidly during the first 60 min and then recached an adsorption equilibrium after 120 min. The regression coefficient (R^2) values (0.783–0.984) of the pseudo-second-order adsorption kinetic rate were superior to those of the pseudo-first-order kinetic rate (0.619–0.974) for Cd^{2+} (II) adsorption. Furthermore, the theoretical and experimental values of q_e were close for pseudo-second-order adsorption kinetics, indicating that the pseudo-second-order model fits well with the experimental adsorption data. These results suggest that the absorption process of Cd^{2+} on FBM and fishbone-derived biochar is controlled by the pseudo-second-order model and support the idea that the adsorption process is due to chemical adsorption [26,27]. These findings align with previous research, which demonstrated that the absorption of divalent and trivalent metal cations (e.g., Cd^{2+}, Pb^{2+}, Cu^{2+}, and Cr^{3+}) onto absorbents (e.g., fish bones and crayfish shell biochar) conformed to the pseudo-second-order model [28]. Furthermore, the maximum absorption

capacity (q_e) acquired from the pseudo-second-order model exhibited the following order: FBM (6.93 mg·g^{-1}) < B_{200} (8.78 mg·g^{-1}) < B_{400} (13.3 mg·g^{-1}) < B_{800} (19.7 mg·g^{-1}) < B_{600} (34.7 mg·g^{-1}), indicating that high-temperature pyrolysis enhanced the Cd^{2+}-adsorption capacity of FBM, with the best pyrolysis temperature being 600 °C.

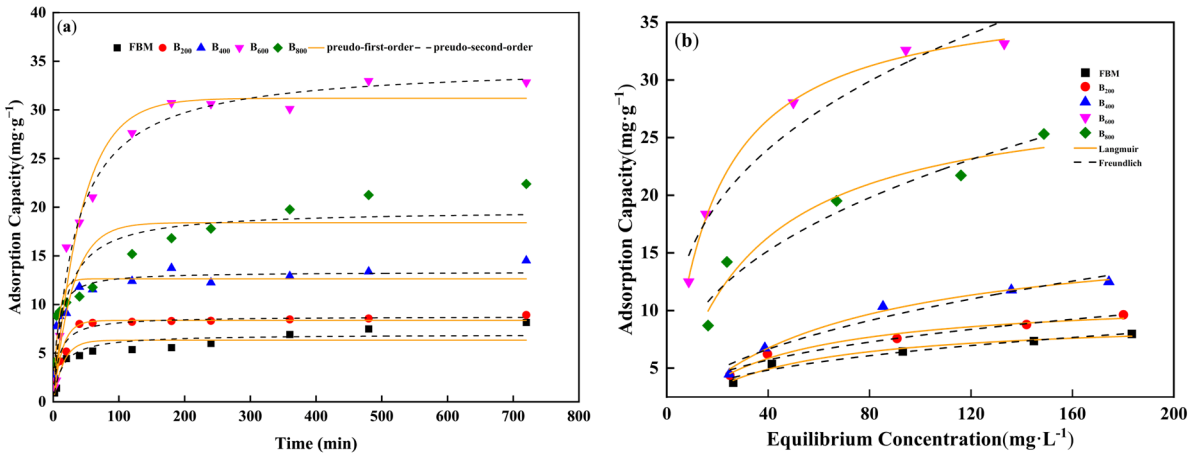

(**a**) (**b**)

Figure 3. Kinetics and isotherm models describing the Cd^{2+} adsorption: (**a**) Fitting results of the pseudo-first-order and pseudo-second-order kinetics model fitting curves for Cd^{2+} adsorption; (**b**) Fitting results of the Langmuir and Freundlich isotherm models for Cd^{2+} adsorption. FBM represents fishbone; B_{200}, B_{400}, B_{600}, and B_{800} represent fishbone biochar prepared at 200 °C, 400 °C, 600 °C, and 800 °C, respectively.

Table 3. The constants of pseudo-first-order and pseudo-second-order kinetics models for Cd adsorption.

	C_0 (mg/L)	*q*e, Exp (mg/g)	Pseudo-First-Order Model			Pseudo-Second-Order Model		
			*q*e, Cal (mg/g)	k_1 (1/min)	R^2	*q*e, Cal (mg/g)	k_2 (g/(mg·min))	
FBM	250	8.163	6.3312	0.0641	0.7823	6.9282	0.0109	0.8635
B_{200}	250	8.926	8.3675	0.0738	0.8966	8.7806	0.0139	0.9406
B_{400}	250	14.518	12.638	0.1254	0.8446	13.346	0.0134	0.9270
B_{600}	250	32.834	31.199	0.0230	0.9747	34.696	0.0009	0.9841
B_{800}	250	22.383	18.413	0.0343	0.6192	19.702	0.0029	0.7830

Note: FBM represents fishbone; B_{200}, B_{400}, B_{600}, and B_{800} represent fishbone biochar prepared at 200 °C, 400 °C, 600 °C, and 800 °C, respectively.

3.2.2. Adsorption Isotherms

Figure 3b presents the fitting results of the Langmuir and Freundlich isotherm models for Cd^{2+} adsorption on FBM and fishbone-derived biochar. The adsorption capacity of Cd^{2+} for FBM and fishbone-derived biochar increased rapidly with the increasing equilibrium concentration at lower Cd^{2+} concentrations and slowly at higher Cd^{2+} concentrations. The R^2 values for the Langmuir absorption isotherm ranged from 0.9413 to 0.9892, which were higher than those for the Freundlich absorption isotherm (0.9236–0.9623) (Table 4). These findings suggest that the Langmuir absorption isotherm model might more accurately describe the Cd^{2+} adsorption on FBM and fishbone-derived biochar and that the Cd^{2+} adsorption on FBM and fishbone-derived biochar could be considered as a single-layer adsorption process [29]. In addition, according to the fitting results of the Langmuir absorption isotherm model (Table 4), the maximum Cd^{2+}-adsorption capacities (q_m) of FBM and fishbone-derived biochar were ranked as follows: FBM (9.28 mg·g^{-1}) < B_{200} (11.2 mg·g^{-1}) < B_{400} (17.2 mg·g^{-1}) < B_{800} (37.8 mg·g^{-1}) < B_{600} (29.3 mg·g^{-1}), further confirming that pyrolysis enhanced the Cd^{2+}-adsorption capacity of FBM, particularly at the temperature of 600 °C. Furthermore, the dimensionless separation factor (R_L) is

regarded as a critical parameter for expressing the feasibility of the Langmuir absorption isotherm [30]. In the present study, R_L was all found to be within 0 and 1, indicating that Cd^{2+} adsorption is a favorable process [31]. Furthermore, 1/n was employed to predict the sorption system's thermodynamic adaptability, and K_F reflects the adsorption capacity of adsorbents. The values of 1/n for FBM and fishbone-derived biochar are all between 0 and 1 (Table 4), implying that chemical adsorption occurred for the Cd^{2+} adsorbents [32]. The K_F values of B_{600} and B_{800} (7.4522 $mg{\cdot}g^{-1}$ $(L{\cdot}g^{-1})^{1/n}$ and 3.7115 $mg{\cdot}g^{-1}$ $(L{\cdot}g^{-1})^{1/n}$, respectively) are significantly greater than those of FBM (1.4075 $mg{\cdot}g^{-1}$ $(L{\cdot}g^{-1})^{1/n}$), showing that the fishbone-derived biochar pyrolyzed at higher temperatures has a stronger affinity for Cd^{2+} than FBM.

Table 4. The constants of the Langmuir and Freundlich isotherm models for Cd adsorption; separation factor of Langmuir isotherm fitting for Cd adsorption.

Isotherm Model	Constants	Sorbents				
		FBM	**B_{200}**	**B_{400}**	**B_{600}**	**B_{800}**
Langmuir	q_m ($mg{\cdot}g^{-1}$)	9.284	11.2267	17.194	37.799	29.267
	K_L ($L{\cdot}mg^{-1}$)	0.0281	0.0271	0.0161	0.0591	0.0316
	R^2	0.9656	0.9650	0.9892	0.9892	0.9413
	R_L	0.1511–0.5426	0.1558–0.5516	0.2370–0.6743	0.0780–0.3606	0.3876–3.7115
Freundlich	K_F ($mg{\cdot}g^{-1}$ $(L{\cdot}g^{-1})^{1/n}$)	1.4075	1.5791	1.2211	7.4522	0.2404
	n	2.9957	2.8729	2.1786	3.1546	0.1742
	R^2	0.9479	0.9623	0.9441	0.9362	0.1366

Note: FBM represents fishbone; B_{200}, B_{400}, B_{600}, and B_{800} represent fishbone biochar prepared at 200 °C, 400 °C, 600 °C, and 800 °C, respectively.

3.2.3. Influence of Initial pH Value on Cd^{2+} Adsorption

The initial solution pH is a critical parameter in the adsorption process because it influences the solubility and speciation of metal ions, the charged properties of the adsorbent surface, and the state of the absorbent functional groups [33]. As previously mentioned, hydroxyapatite (HPA), the major component of fish bone, may dissolve at a pH below 3 [34]. Concurrently, Cd primarily exists as Cd^{2+} in solution with a pH below 8, while at a pH exceeding 8, the Cd^{2+} in solution can form hydroxides, such as $Cd(OH)^+$ or $Cd(OH)_2$, leading to precipitation [24]. Therefore, to avoid adsorbent dissolution and Cd precipitation, the initial solution pH was set between 3 and 8 for absorption. Figure 4 presents the effect of initial solution pH values on the adsorption capacity of Cd^{2+} on fishbone-derived biochar. The adsorption capacity of Cd on FBM and fishbone-derived biochar increased dramatically in the pH range of 3–6, subsequently steadily stabilizing at pH above 6. The total increase in adsorption capacities of Cd on FBM and fishbone-derived biochar (B_{200}, B_{400}, B_{600}, and B_{800}) were 5.08 $mg{\cdot}g^{-1}$, 7.64 $mg{\cdot}g^{-1}$, 11.93 $mg{\cdot}g^{-1}$, 17.78 $mg{\cdot}g^{-1}$, and 13.55 $mg{\cdot}g^{-1}$, respectively, indicating that pH has a significant effect on the adsorption of Cd^{2+} on fishbone-derived biochar. The following reasons can be used to explain these effects: First, the competition between Cd^{2+} and an abundance of hydrogen ions (H^+) in the lower pH solution results in a reduction of adsorption capacity for Cd^{2+}. Second, in a higher pH solution, the concentration of H^+ decreases with increasing pH. Subsequently, the surfaces of the absorbents become negatively charged, thereby enhancing the adsorption capacity for Cd^{2+} [11].

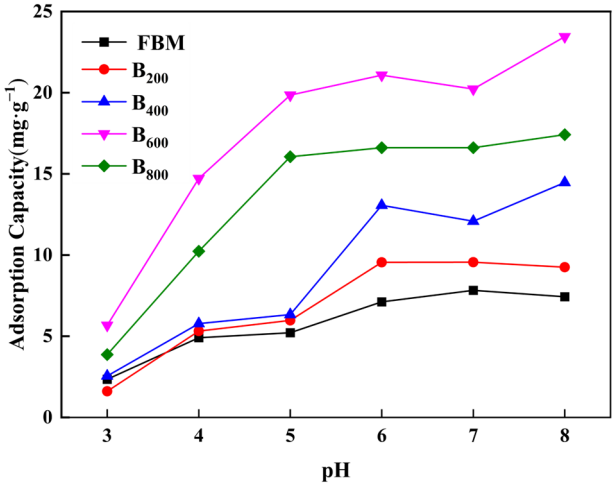

Figure 4. The adsorption capacity of Cd^{2+} by fishbone-derived biochar under different initial pH values. FBM represents fishbone; B_{200}, B_{400}, B_{600}, and B_{800} represent fishbone biochar prepared at 200 °C, 400 °C, 600 °C, and 800 °C, respectively.

3.3. Adsorption Mechanisms

In the present study, high-temperature pyrolysis enhanced the Cd^{2+} adsorption capacity of FBM, with the optimal pyrolysis temperature being 600 °C. The kinetic data of FBM and fishbone-derived biochar for Cd^{2+} were in alignment with the pseudo-second-order model, and the maximum Cd^{2+}-adsorption capacity of FBM and fishbone-derived biochar (B_{200}, B_{400}, B_{600}, and B_{800}) were 9.28 $mg \cdot g^{-1}$, 11.2 $mg \cdot g^{-1}$, 17.2 $mg \cdot g^{-1}$, 37.8 $mg \cdot g^{-1}$, and 29.3 $mg \cdot g^{-1}$, respectively, when the initial Cd^{2+} concentration was 200 $mg \cdot L^{-1}$. Furthermore, the SEM–EDS results further corroborate that Cd^{2+} successfully adsorbed onto FBM and fishbone-derived biochar (Figure 5 and Table 5). The adsorption mechanisms involved in this process are as follows: First, fishbone contains approximately 70% mineral components (primarily HAP), and the SEM–EDS results of FBM and fishbone-derived biochar used in the present study support this finding (Tables 1 and 5) [19]. Previous research has demonstrated the existence of an ion-exchange reaction between heavy metal ions and Ca^{2+} ions of HAP [35], and that the adsorption mechanism of Cu^{2+} on HAP could be described as follows:

$$HAP_{(Surface)} - Ca_{10}(PO_4)_6 \cdot (OH)_2 + xCu + 2xCl^- \rightarrow Ca_{(10-X)} \cdot Cu_x(PO_4)_6(OH)_2 + xCa^{2+} + 2xCl^-$$

Table 5. Element compositions of FBM-Cd, B_{200}-Cd, B_{400}-Cd, and B_{600}-Cd determined by SEM–EDS.

Element (wt %)	FBM-Cd	B_{200}-Cd	B_{400}-Cd	B_{600}-Cd	B_{800}-Cd
Ca	62.83	45.42	41.60	31.92	49.34
Na	0.04	0.40	0.78	0.29	0.61
C	7.35	9.55	12.45	13.47	9.58
O	13.64	16.88	11.10	10.62	5.71
Si	3.29	8.53	9.54	13.48	5.70
Cd	12.85	19.21	22.39	30.21	24.06
Al	ND	ND	2.13	ND	ND

Note: ND means no detection. FBM-Cd represents Cd-absorbed fishbone; B_{200}-Cd, B_{400}-Cd, B_{600}-Cd, and B_{800}-Cd represent Cd-absorbed fishbone biochar that was prepared at 200 °C, 400 °C, 600 °C, and 800 °C, respectively.

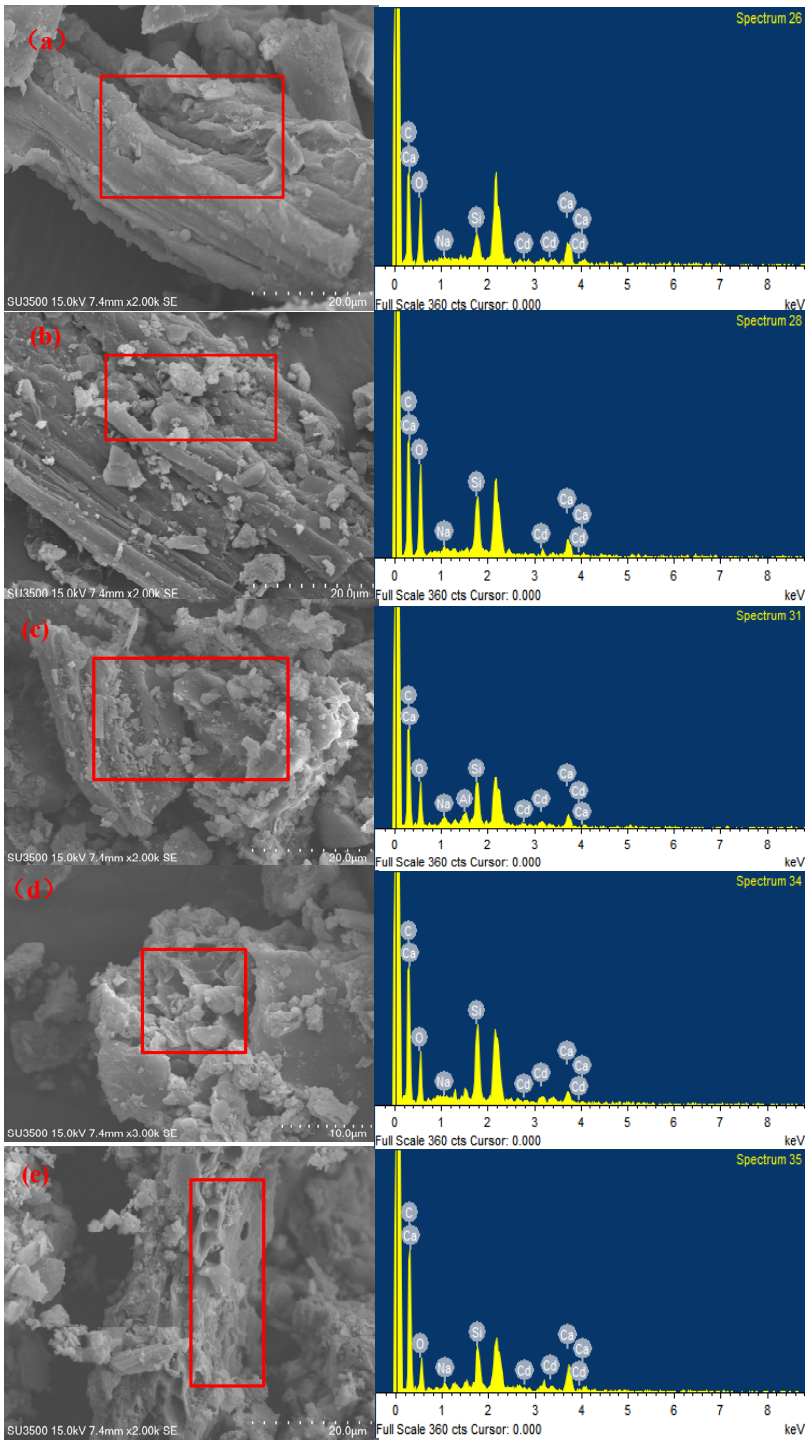

Figure 5. SEM–EDS spectra of (**a**) FBM-Cd, (**b**) B_{200}-Cd, (**c**) B_{400}-Cd, (**d**) B_{600}-Cd, and (**e**) B_{800}-Cd. FBM-Cd represents Cd-absorbed fishbone; B_{200}-Cd, B_{400}-Cd, B_{600}-Cd, and B_{800}-Cd represent Cd-absorbed fishbone biochar that was prepared at 200 °C, 400 °C, 600 °C, and 800 °C, respectively.

Given that Cd^{2+} and Cu^{2+} are both bivalent cations, we hypothesized that the adsorption process of Cd^{2+} on HAP was comparable to that of Cu^{2+}. Second, the absorbents FBM and fishbone-derived biochar used in the present study exhibit a primarily microporous size distribution with a trace of mesopores (Figure 2a), and thus Cd^{2+} in solution can be transferred through mesopores and adsorbed in micropores. Furthermore, FBM and fishbone-derived biochar have an abundance of surface functional groups, including -OH, $-CH_2$, PO_4^{3-}, and C=O (Figure 1a). According to the FTIR results before and after B_{600}

adsorption of Cd^{2+}, it can be seen that there are many band shifts, indicating that a variety of functional groups participate in the adsorption process of Cd^{2+}. A comparison between the FTIR spectra of B_{600} and Cd-absorbed biochar (B_{600}-Cd) showed a significant increase in the intensity of peaks at 3200 cm^{-1}, 1460 cm^{-1}, 1090 cm^{-1}, and 470 cm^{-1} (Figure 1c), indicating the critical role of -OH and PO_4^{3-} functional groups on the biochar surface for Cd^{2+} sorption. The adsorption of Cd^{2+} on FBM and fishbone-derived biochar might occur through the complexation of Cd^{2+} with these functional groups on the surface of biochar. Therefore, based on the above findings and analysis, the Cd^{2+} adsorption process by FBM and fishbone-derived biochar was a combination of physical and chemical adsorption [35].

Previous research has demonstrated that the structure and properties of biochar are influenced by the pyrolysis temperature [36]. At first, as the pyrolysis temperature increased, the surface functional groups on biochar became less diverse and dense because the oxygen-containing functional groups were released [37]. Compared to the FTIR spectrum of FBM, the intensity of peaks at 1090 cm^{-1} and 1030 cm^{-1} in the FTIR spectra of fishbone-derived biochar (B_{200}, B_{400}, B_{600}, and B_{800}) increased with the increased pyrolysis temperature (Figure 1b), indicating that the diversity and density of the surface functional groups of FBM and fishbone-derived biochar were altered by high-temperature pyrolysis. Moreover, a comparison of the FTIR spectra of B_{600} and Cd-absorbed biochar (B_{600}-Cd) showed a significant increase in the intensity of peaks at 3200 cm^{-1}, 1460 cm^{-1}, 1090 cm^{-1}, and 470 cm^{-1} (Figure 1c), indicating the critical role of -OH and PO_4^{3-} functional groups on the biochar surface for Cd^{2+} adsorption. In addition, in the current study, high-temperature pyrolysis did not significantly affect the specific surface area of the fishbone-derived biochar. Conversely, the pore volume of the fishbone-derived biochar grew significantly as the pyrolysis temperature increased (Table 1). Moreover, Figure 5a shows that there were gullies and cracks on the surface of FBM, with no obvious pore structure. Thus, we speculated that surface pore filling was one of the mechanisms involved in Cd^{2+} adsorption on fishbone-derived biochar. Researchers have also found that the sorption of Cd on the palm oil mill sludge biochar pyrolyzed at a higher temperature occurred most likely due to surface pore filling [38]. Additionally, increasing the pyrolysis temperature to 600 °C significantly increased the alkaline functional groups and aromaticity of fishbone-derived biochar. This suggested that the chemisorption of mineral elements precipitated on the surface of biochar with Cd may be relevant. Also, high pyrolysis temperatures could degrade the surface functional groups, which would reduce the adsorbed amount of Cd^{2+} on the surface functional groups of absorbents. Additionally, in the current study, the pH_{ZPC} values for B_{600} and B_{800} were greater than 8, indicating that there are no significant variations in the adsorbed amount of Cd^{2+} by mineral components precipitated on the surface of biochar. Overall, the primary absorption mechanisms of FBM for Cd^{2+} in solution were associated with the ion-exchange reaction between Cd^{2+} and HAP on the FBM surface and Cd^{2+} complexation with functional groups on the surface of FBM. At lower pyrolysis temperatures (200–400 °C), the primary absorption mechanisms for fishbone-derived biochar were pore filling and the ion-exchange reaction between Cd^{2+} and HAP on the surface of biochar. At higher pyrolysis temperatures (600–800 °C), the primary absorption mechanisms for fishbone-derived biochar were pore filling and precipitation of mineral elements with Cd^{2+} on the surface of biochar.

4. Conclusions

In this study, FBW and fishbone-derived biochar obtained at different pyrolysis temperatures were used to test their adsorption properties for Cd^{2+} in aqueous solution. The results showed that high-temperature pyrolysis enhanced the Cd^{2+}-adsorption capacity of fishbone (FBM), with the optimal pyrolysis temperature being 600 °C. High-temperature pyrolysis could optimize the pore structure and specific surface area of FBM. The kinetic data of FBM and fishbone-derived biochar for Cd^{2+} were in better alignment with the pseudo-second-order model, and the maximum Cd^{2+}-adsorption capacity of fishbone-derived biochar was 37.8 $mg \cdot g^{-1}$, when the initial Cd^{2+} concentration was 200 $mg \cdot L^{-1}$.

Furthermore, the adsorption isotherms of FBM and fishbone-derived biochar for Cd^{2+} were better in accordance with the Langmuir model. Thermodynamic analysis demonstrated that the adsorption process was monolayer and favorable adsorption. Additionally, the potential adsorption mechanisms of Cd^{2+} on fishbone-derived biochar may be classified into four parts: pore filling, ion exchange, complexation with oxygen functional groups, and precipitation with minerals on the biochar surface. Our findings indicate that fishbone-derived biochar has significant potential for removing Cd^{2+} from aqueous solutions and increasing the abandoned fishbone resource efficiency.

Author Contributions: Writing—original draft, N.P.; conceptualization, methodology, software, W.L.; writing—review and editing, Q.H. and Y.S. All authors have read and agreed to the published version of the manuscript.

Funding: This research was funded by the Innovation Program of Chinese Academy of Agricultural Sciences, grant number CAAS–CSGLCA–202302.

Data Availability Statement: The data that support the findings of this study are available from the corresponding author upon reasonable request.

Conflicts of Interest: The authors declare no conflicts of interest.

References

1. Teng, D.; Zhang, B.; Xu, G.; Wang, B.; Mao, K.; Wang, J.; Sun, J.; Feng, X.; Yang, Z.; Zhang, H. Efficient removal of Cd(II) from aqueous solution by pinecone biochar: Sorption performance and governing mechanisms. *Environ. Pollut.* **2020**, *265*, 115001. [CrossRef] [PubMed]
2. Si, H.C.; Yuen, L.C.; Si, L.N.; Adeline, S.Y.T. Influence of Dyes on Metal Removal: A Study Using Live and Dead Cells of Penicillium simplicissimum in Single-Metal and Dye-Metal Mixtures. *Water Air Soil Poll.* **2018**, *229*, 271.
3. Yan, Y.L.; Sam, S.S.L.; Jonathan, W.C.W. Removal of Cd(II) from aqueous solutions using plant-derived biochar: Kinetics, isotherm and characterization. *Bioresour. Technol. Rep.* **2019**, *8*, 100323.
4. Abdin, Y.; Usman, A.; Ok, Y.S.; Tsang, Y.F.; Al-Wabel, M. Competitive sorption and availability of coexisting heavy metals in mining-contaminated soil: Contrasting effects of mesquite and fishbone biochars. *Environ. Res.* **2020**, *181*, 108846. [CrossRef]
5. Liu, P.; Rao, D.; Zou, L.; Teng, Y.; Yu, H. Capacity and potential mechanisms of Cd(II) adsorption from aqueous solution by blue algae-derived biochars. *Sci. Total Environ.* **2021**, *767*, 145447. [CrossRef] [PubMed]
6. Hu, X.; Cao, J.; Yang, H.; Li, D.; Qiao, Y.; Zhao, J.; Zhang, Z.; Huang, L. Pb^{2+} biosorption from aqueous solutions by live and dead biosorbents of the hydrocarbon-degrading strain Rhodococcus sp. HX-2. *PLoS ONE* **2020**, *15*, e0226557. [CrossRef]
7. Seyed, A.Z.; Robiah, Y.; Samsuri, A.W.; Mohd Salleh, M.A.; Bahareh, A. Removal of zinc from aqueous solution by optimized oil palm empty fruit bunches biochar as low cost adsorbent. *Bioinorg. Chem. Appl.* **2017**, *1*, 7914714.
8. Iqbal, J.; Shah, N.S.; Sayed, M.; Niazi, N.K.; Imran, M.; Khan, J.A.; Khan, Z.U.H.; Hussien, A.G.S.; Polychronopoulou, K.; Howari, F. Nano-zerovalent manganese/biochar composite for the adsorptive and oxidative removal of Congo-red dye from aqueous solutions. *J. Hazard Mater.* **2021**, *403*, 123854. [CrossRef]
9. Idrees, M.; Batool, S.; Hussain, Q.; Ullah, H.; Al-Wabel, M.I.; Ahmad, M.; Kong, J. High-efficiency remediation of cadmium (Cd^{2+}) from aqueous solution using poultry manure- and farmyard manure-derived biochars. *Separ. Sci. Technol.* **2016**, *51*, 2307–2317. [CrossRef]
10. Sun, T.; Xu, Y.; Sun, Y.; Wang, L.; Liang, X.; Jia, H. Crayfish shell biochar for the mitigation of Pb contaminated water and soil: Characteristics, mechanisms, and applications. *Environ. Pollut.* **2021**, *271*, 116308. [CrossRef]
11. Qiu, B.; Tao, X.; Wang, H.; Li, W.; Ding, X.; Chu, H. Biochar as a low-cost adsorbent for aqueous heavy metal removal: A review. *J. Anal. Appl. Pyrol.* **2021**, *155*, 105081. [CrossRef]
12. Yang, T.; Xu, Y.; Huang, Q.; Sun, Y.; Liang, X.; Wang, L.; Qin, X.; Zhao, L. Adsorption characteristics and the removal mechanism of two novel Fe-Zn composite modified biochar for Cd(II) in water. *Bioresour. Technol.* **2021**, *333*, 125078. [CrossRef] [PubMed]
13. Huang, F.; Gao, L.; Wu, R.; Wang, H.; Xiao, R. Qualitative and quantitative characterization of adsorption mechanisms for Cd^{2+} by silicon-rich biochar. *Sci. Total Environ.* **2020**, *731*, 139163. [CrossRef] [PubMed]
14. Liu, X.; Steele, J.C.; Meng, X. Usage, residue, and human health risk of antibiotics in Chinese aquaculture: A review. *Environ. Pollut.* **2017**, *223*, 161–169. [CrossRef] [PubMed]
15. Valencia Junca, M.A.; Valencia, C.; Florez Lopez, E.; Delgado-Ospina, J.; Zapata, P.A.; Solano, M.; Grande Tovar, C.D. Chitosan Beads Incorporated with Essential Oil of Thymus capitatus: Stability Studies on Red Tilapia Fillets. *Biomolecules* **2019**, *9*, 458. [CrossRef]
16. Qin, J.; Wang, Z.; Wang, X.; Shi, W. Effects of microwave time on quality of grass carp fillets processed through microwave combined with hot-air drying. *Food Sci. Nutr.* **2020**, *8*, 4159–4171. [CrossRef]
17. Cao, L.; Naylor, R.; Henriksson, P.; Leadbitter, D.; Metian, M.; Troell, M.; Zhang, W. China's aquaculture and the world's wild fisheries. *Science* **2015**, *347*, 133–135. [CrossRef]

18. Mo, W.Y.; Man, Y.B.; Wong, M.H. Use of food waste, fish waste and food processing waste for China's aquaculture industry: Needs and challenge. *Sci. Total Environ.* **2018**, *613*, 635–643. [CrossRef]
19. Dimovic, S.; Smiciklas, I.; Plecas, I.; Antonovic, D.; Mitric, M. Comparative study of differently treated animal bones for Co^{2+} removal. *J. Hazard Mater.* **2009**, *164*, 279–287. [CrossRef]
20. Wan, K.; Huang, L.; Yan, J.; Ma, B.; Huang, X.; Luo, Z.; Zhang, H.; Xiao, T. Removal of fluoride from industrial wastewater by using different adsorbents: A review. *Sci. Total Environ.* **2021**, *773*, 145535. [CrossRef]
21. Hernandez-Cocoletzi, H.; Salinas, R.A.; Aguila-Almanza, E.; Rubio-Rosas, E.; Chai, W.S.; Chew, K.W.; Mariscal-Hernandez, C.; Show, P.L. Natural hydroxyapatite from fishbone waste for the rapid adsorption of heavy metals of aqueous effluent. *Environ. Technol. Innov.* **2020**, *20*, 101109. [CrossRef]
22. Sun, T.; Pei, P.G.; Sun, Y.B.; Xu, Y.M.; Jia, H.T. Performance and mechanism of As(III/V) removal from aqueous solution by novel positively charged animal-derived biochar. *Sep. Purif. Technol.* **2022**, *290*, 120836. [CrossRef]
23. Ran, J.; Hu, J.; Sun, G.; Chen, S.; Chen, L.; Shen, X.; Tong, H. Comparisons between gelatin-tussah silk fibroin/hydroxyapatite and gelatin-Bombyx mori silk fibroin/hydroxyapatite nano-composites for bone tissue engineering. *RSC Adv.* **2015**, *5*, 76526–76537. [CrossRef]
24. Li, H.; Dong, X.; Da Silva, E.B.; de Oliveira, L.M.; Chen, Y.; Ma, L.Q. Mechanisms of metal sorption by biochars: Biochar characteristics and modifications. *Chemosphere* **2017**, *178*, 466–478. [CrossRef]
25. Zolfi Bavariani, M.; Ronaghi, A.; Ghasemi, R. Influence of Pyrolysis Temperatures on FTIR Analysis, Nutrient Bioavailability, and Agricultural use of Poultry Manure Biochars. Commun. *Soil Sci. Plan.* **2019**, *50*, 402–411. [CrossRef]
26. Kara, A.; Demirbel, E.; Tekin, N.; Osman, B.; Besirli, N. Magnetic vinylphenyl boronic acid microparticles for Cr(VI) adsorption: Kinetic, isotherm and thermodynamic studies. *J. Hazard Mater.* **2015**, *286*, 612–623. [CrossRef] [PubMed]
27. Inyang, H.I.; Onwawoma, A.; Bae, S. The Elovich equation as a predictor of lead and cadmium sorption rates on contaminant barrier minerals. *Soil. Till. Res.* **2016**, *155*, 124–132. [CrossRef]
28. Bing, L.; Lan, Y.; Wang, C.Q.; Zhang, Q.P.; Liu, Q.C.; Li, Y.D.; Rui, X. Adsorption of Cd(II) from aqueous solutions by rape straw biochar derived from different modification processes. *Chemosphere* **2017**, *175*, 332–340.
29. Cleide, S.T.A.; Ione, L.S.A.; Hélen, C.R.; Suzana, M.L.O.M.; José, J.L.L.; Túlio, N.D.M. Elucidation of mechanism involved in adsorption of Pb(II) onto lobeira fruit (*Solanum lycocarpum)* using Langmuir, Freundlich and Temkin isotherms. *Microchem. J.* **2018**, *137*, 348–354.
30. Lin, L.; Qiu, W.; Wang, D.; Huang, Q.; Song, Z.; Chau, H.W. Arsenic removal in aqueous solution by a novel Fe-Mn modified biochar composite: Characterization and mechanism. *Ecotoxicol. Environ. Saf.* **2017**, *144*, 514–521. [CrossRef]
31. Li, S.; Barreto, V.; Li, R.; Chen, G.; Hsieh, Y.P. Nitrogen retention of biochar derived from different feedstocks at variable pyrolysis temperatures. *J. Anal. Appl. Pyrol.* **2018**, *133*, 136–146. [CrossRef]
32. Hasanpour, M.; Hatami, M. Application of three dimensional porous aerogels as adsorbent for removal of heavy metal ions from water/wastewater: A review study. *Adv. Colloid Interfac.* **2020**, *284*, 102247. [CrossRef] [PubMed]
33. Mnasri-Ghnimi, S.; Frini-Srasra, N. Removal of heavy metals from aqueous solutions by adsorption using single and mixed pillared clays. *Appl. Clay. Sci.* **2019**, *179*, 105151. [CrossRef]
34. Jung, K.W.; Lee, S.Y.; Choi, J.W.; Lee, Y.J. A facile one-pot hydrothermal synthesis of hydroxyapatite/biochar nanocomposites: Adsorption behavior and mechanisms for the removal of copper (II) from aqueous media. *Chem. Eng. J.* **2019**, *369*, 529–541. [CrossRef]
35. Kizilkaya, B.; Tekinay, A.A.; Dilgin, Y. Adsorption and removal of Cu (II) ions from aqueous solution using pretreated fish bones. *Desalination* **2010**, *264*, 37–47. [CrossRef]
36. Zhao, B.; O'Connor, D.; Zhang, J.; Peng, T.; Shen, Z.; Tsang, D.C.W.; Hou, D. Effect of pyrolysis temperature, heating rate, and residence time on rapeseed stem derived biochar. *J. Clean. Prod.* **2018**, *174*, 977–987. [CrossRef]
37. Wystalska, K.; Kwarciak-Kozlowska, A. The Effect of Biodegradable Waste Pyrolysis Temperatures on Selected Biochar Properties. *Materials* **2021**, *14*, 1644. [CrossRef]
38. Goh, C.L.; Sethupathi, S.; Bashir, M.J.; Ahmed, W. Adsorptive behaviour of palm oil mill sludge biochar pyrolyzed at low temperature for copper and cadmium removal. *J. Environ. Manag.* **2019**, *237*, 281–288. [CrossRef]